Multilayered Inclusions in Locally Resonant Metamaterials: Two-Dimensional Versus Three-Dimensional Modeling

Anastasiia O. Krushynska[1]
Department of Physics,
University of Turin,
Turin 10125, Italy
e-mail: akrushynska@gmail.com

Marco Miniaci
Laboratoire Ondes et Milieux Complexes,
University of Le Havre,
Le Havre 76600, France
e-mail: marco.miniaci@gmail.com

Varvara G. Kouznetsova
Department of Mechanical Engineering,
Eindhoven University of Technology,
Eindhoven 5600MB, The Netherlands
e-mail: v.g.kouznetsova@tue.nl

Marc G. D. Geers
Professor
Department of Mechanical Engineering,
Eindhoven University of Technology,
Eindhoven 5600MB, The Netherlands
e-mail: m.g.d.geers@tue.nl

Locally resonant metamaterials (LRMs) controlling low-frequency waves due to resonant scattering are usually characterized by narrow band gaps (BGs) and a poor wave filtering performance. To remedy this shortcoming, multiresonant metamaterial structures with closely located BGs have been proposed and widely studied. However, the analysis is generally limited to two-dimensional (2D) structures neglecting the finite height of any real resonator. The aim of this paper is the comparison of the wave dispersion for two- and three-dimensional (3D) metamaterial models and evaluation of the applicability ranges of 2D results. Numerical study reveals that dual-resonant structures with cylindrical inclusions possess only a single (compared to two in the 2D case) BG for certain height-to-width ratios. In contrast, the wave dispersion in metamaterials with multiple spherical resonators can be accurately evaluated using a 2D approximation, enabling a significant simplification of resource-consuming 3D models. [DOI: 10.1115/1.4035307]

1 Introduction

Mechanical metamaterials with unusual dynamic behavior are artificially structured composites that exhibit absolute BGs—frequency regions, within which wave propagation is inhibited. In LRMs, the BGs are opened due to resonant scattering of elastic waves from (non)periodic inhomogeneities on a subwavelength scale. This important characteristic allows to control and manipulate waves with wavelengths up to two-orders of magnitude larger than the dimensions of resonators. This opens up many promising applications, including subwavelength imaging [1], seismic wave abatement [2], and acoustic cloaking [3], to name a few. However, local resonances usually result in narrow BGs with poor attenuation performance of LRMs.

Many efforts have been done to broaden BGs in LRMs. Among these, a promising strategy is designing structures with multiple local resonators. Larabi et al. [4] proposed multilayered cylindrical resonators with coaxial alternating shells of soft and hard materials and showed that closely located BGs can be overlapped by adjusting the resonator geometry. Later, the performance of a similar LRM was analyzed by using an equivalent mass-in-mass dual-resonator model for blast-wave impact mitigation [5]. Chen et al. [6] recently extended this model to incorporate viscous effects of constitutive materials. Zhu et al. [7] investigated the wave attenuation abilities of a chiral LRM with multiple resonators both analytically and experimentally. Similarly, for the acoustic field, Elford et al. [8] proposed an LRM of a Matryoshka-like configuration of slotted cylinders with numerous BGs in the subwavelength frequency regime. Finally, the concept of multiple local resonators was exploited by Krödel et al. [9] to propose large-scale metamaterials for protecting civil infrastructures from earthquake excitations.

In all the mentioned studies, the resonators have a cylindrical shape and are assumed to have an infinite or semi-infinite length enabling 2D analysis. Actual resonators always have finite sizes, e.g., in slab metamaterial geometries. Hence, one objective of this study is to investigate the effect of the finite height of resonators on the attenuation performance of metamaterials with multiple resonators. A similar study for slab phononic crystals with Bragg-type band gaps [10] revealed that absolute BGs only exist for certain thickness to lattice size ratios. To the best of our knowledge, such an analysis on LRMs has not been performed yet. In addition, this letter aims at generalizing a well-known conclusion [11] that a simplified 2D model can account for wave dispersion in a metamaterial with a single-coated spherical inclusion to the case of multilayered spherical resonators.

2 Cylindrical Resonators

Let us consider an LRM with multilayered co-axial resonators of a cylindrical shape and height h, embedded in a solid matrix in a periodic square array. The representative unit cell and its cross section are shown in Fig. 1 along with relevant geometrical parameters (in millimeter). The epoxy matrix is characterized by Young's modulus $E = 3.6$ GPa, Poisson's ratio $\nu = 0.37$, and mass density $\rho = 1180$ kg/m^3. The central hard core and the thinnest ring are made of tungsten with $E = 411$ GPa, $\nu = 0.28$, and $\rho = 19{,}250$ kg/m^3. The coating layers represented by two wide rings are made of rubber with $E = 150$ kPa, $\nu = 0.4995$, and $\rho = 1300$ kg/m^3. Losses resulting from material dissipation are
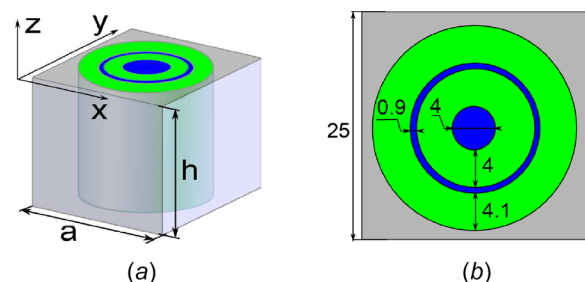

Fig. 1 Schematic representation of the 3D unit cell and its cross section for an LRM with multilayered cylindrical inclusions (the geometrical parameters are given in millimeters)

neglected in order to restrict the attenuation effects to local resonance mechanisms, only. The geometry with thick rubber layers is chosen to reduce computational costs, since the proper resolution for the wavelength in the coating requires a rather fine mesh with at least 4–6 finite elements across the thickness [12].

The 2D structure is analyzed first. In this case, the displacement field $\mathbf{u}_{2D}(x,y) = u_x(x,y)\mathbf{e}_x + u_y(x,y)\mathbf{e}_y + u_z(x,y)\mathbf{e}_z$ and the wave vector $\mathbf{k}_{2D}(x,y) = k_x(x,y)\mathbf{e}_x + k_y(x,y)\mathbf{e}_y$ are confined to the x–y plane. Then, pure transverse (out-of-plane) modes governed by $u_z(x,y)$ and mixed (in-plane) modes described by $u_x(x,y)$, $u_y(x,y)$ can propagate independently. According to the Bloch–Floquet theorem, mechanical fields are periodic in a periodically structured medium that yields the following relations for displacements at the unit cell boundaries [13]:

$$\mathbf{u}_{2D}(x + a_1, y + a_2; k_x, k_y) = \mathbf{u}_{2D}(x,y)\exp[i(\mathbf{k}_{2D} \cdot \mathbf{a})] \quad (1)$$

where $\mathbf{a} = a_x\mathbf{e}_x + a_y\mathbf{e}_y$ is the size of a representative unit cell along the x and y directions. For the considered geometry, $a_x = a_y = a$.

Next, a 3D slab structure of a finite height h is considered with the displacement field $\mathbf{u}_{3D}(x,y,z) = u_x(x,y,z)\mathbf{e}_x + u_y(x,y,z)\mathbf{e}_y + u_z(x,y,z)\mathbf{e}_z$ and the wave vector $\mathbf{k}_{3D}(x,y) = k_x(x,y)\mathbf{e}_x + k_y(x,y)\mathbf{e}_y$. The main difference with the 2D case is that the displacement $\mathbf{u}_{3D}$ varies across three dimensions, in contrast to $\mathbf{u}_{2D}(x,y)$ in the 2D model. Thus, the finite height of the structure and its influence on the local resonance BGs are properly accounted for. The following Bloch conditions are applied at the unit cell lateral boundaries:

$$\mathbf{u}_{3D}(x + a_1, y + a_2, z; k_x, k_y) = \mathbf{u}_{3D}(x,y,z)\exp[i(\mathbf{k}_{2D} \cdot \mathbf{a})] \quad (2)$$

The slab boundary faces at $z = 0$ and $z = h$ are traction-free.

Band structure diagrams for the two cases are usually evaluated for the components of $\mathbf{k}$ along the boundary of the first irreducible Brillouin zone Γ–X–M, see, e.g., Ref. [14] for details. The corresponding frequencies can be calculated by means of the finite-element method. In this study, the simulations have been performed by using a commercial finite-element software. Each unit cell is discretized by finite elements. For in-plane modes, three-node Lagrange triangular linear finite elements available in COMSOL MULTIPHYSICS 4.3 are used under plane strain assumption; for out-of-plane modes, eight-node quadrilateral finite elements are used for the acoustic modal analysis in MSC.Marc Mentat 2010. For the 3D slab geometry, the analysis is performed in COMSOL MULTIPHYSICS 4.3 by using four-node Lagrange tetrahedral linear finite elements.

The results for a coarse mesh agree well with those for a fine mesh (the number of elements is doubled), when at least six finite elements across the thickness of each rubber coating layer are used. Thus, confirming mesh convergence for all the calculated data.

Band diagram for the out-of-plane modes shown in Fig. 2(a) exhibits two local resonance BGs at frequencies between $f = 110$ Hz and $f = 174$ Hz, $f = 212$ and $f = 271$ Hz. The BGs are opened at frequencies, when the stiff parts of the resonator vibrate as rigid bodies out-of-phase with respect to the matrix and each other with maximum displacements in the internal core (Figs. 2(c) and 2(d)). For the in-plane modes, the band diagram shown in Fig. 2(b) has a similar structure with approximately twice the number of pass bands and two BGs between $f = 425$ Hz and $f = 457$ Hz, $f = 618$ Hz and $f = 668$ Hz induced in a similar manner, as described in detail in Ref. [4]. Vibration patterns at the frequencies $f = 185$ Hz and $f = 425$ Hz indicate pure torsional motion, when the core rotates within the coating (Fig. 2(e)) and translational motion of the internal core within the coating (Fig. 2(f)), respectively.

Figure 3(a) shows the band diagram for the LRM[3] with $h = 0.2a$, where $a = 25$ mm is the in-plane unit cell size. The band diagrams for 2D and 3D slab unit cells have a similar structure characterized by the presence of a number of localized modes represented by flat curves. Most of the localized modes in the 3D unit cell have an equivalent mode among the 2D in-plane and out-of-plane modes located at almost the same frequencies. The corresponding vibration patterns indicate the dominant planar or out-of-plane motions at those frequencies. The displacement fields at the high-symmetry point X at frequencies $f = 105$ Hz and $f = 185$ Hz (Figs. 3(b) and 3(c)) resemble the vibration patterns of a 2D out-of-plane mode, which constitutes the bound of the BG, and an in-plane torsional mode, respectively. However, in the band diagram for the 3D case, mixed localized modes also exist without any dominant displacement as the one shown in Fig. 3(d) for the lower BG bound.

The main distinction between the 2D and 3D simulation results is the existence of only one BG in the 3D case extending from 206 Hz to 259 Hz. The BG frequencies correspond to those for the second BG of the 2D out-of-plane modes with the displacement field at the upper bound indicating dominant out-of-plane motions (Fig. 3(e)). However, as mentioned above, the lower bound of the BG is formed by a mixed mode with strong planar displacements.

In the 3D case, the BG size appears to be strongly dependent on the slab height, as also observed for phononic structures [10]. The performed analysis reveals that as the height of the slab increases, the BG decreases in width and shifts to higher frequencies. A gap map displaying the dependence of BG frequencies on the height
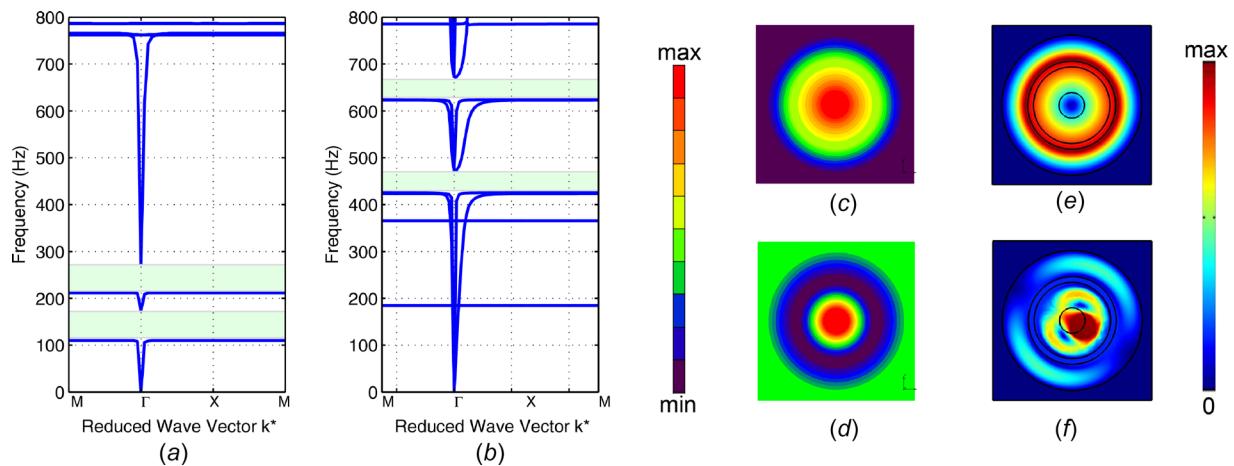

Fig. 2 Band diagrams for 2D out-of-plane (a) and in-plane (b) modes in the LRM with infinite value of h. Vibration patterns of the 2D localized out-of-plane—(c) $f = 110$ Hz and (d) $f = 212$ Hz—and in-plane modes—(e) $f = 185$ Hz and (f) $f = 425$ Hz.
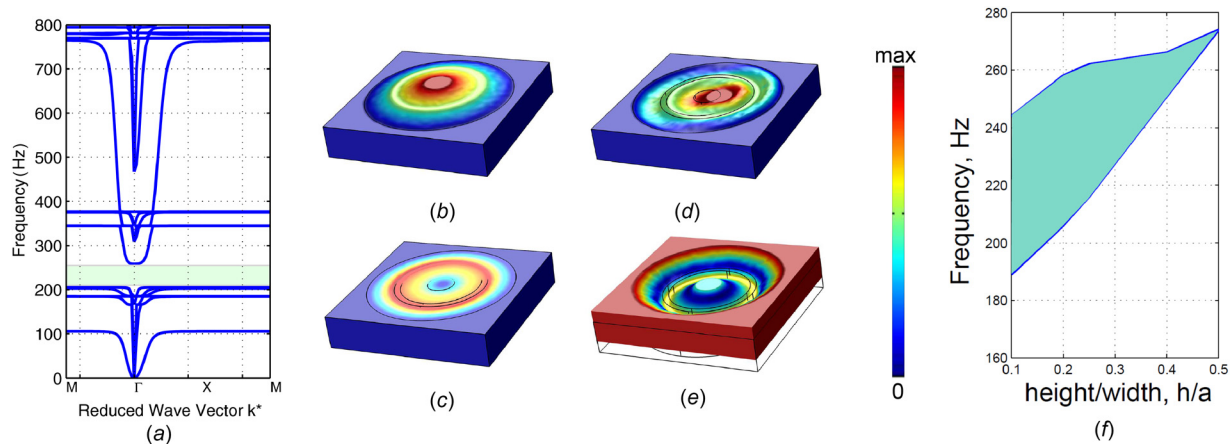
Fig. 3 (*a*) Band diagram of a 3D slab of height *h* = 0.2*a*. (*b*)–(*e*) Vibration patterns of the localized modes for the slab with height *h* = 0.2*a*. (*f*) Complete band gap frequencies as a function of the unit cell height-to-width ratio *h/a*. (*b*) *f* = 105 Hz, (*c*) *f* = 185 Hz, (*d*) *f* = 206 Hz, and (*e*) *f* = 259 Hz.

of the unit cell is shown in Fig. 3(*f*). The BG is completely closed for *h/a* = 0.5. For values between *h/a* = 0.5 and *h/a* = 2, no BG can be observed in the considered frequency range. Note that for larger ratios of *h/a*, the simulations become computationally very demanding, since the number of finite elements increases considerably.

Similar dependence of the BG size on the *h/a* ratio (Fig. 3(*f*)) has been observed for phononic structures [10]. However, in the case of LRMs, the band gap closing occurs due to the appearance of 3D mixed modes characterized by coupled in-plane and out-of-plane displacements as opposed to higher-order slab modes in phononic structures. Thus, the conditions for the BG opening are satisfied only for *h/a* < 0.5 in the low-frequency range. As the value of *h/a* increases, more mixed modes appear, and the lower band gap border (Fig. 3(*d*)) is shifted to higher frequencies and eventually closes the BG at *h/a* = 0.5.

Finally, it can be concluded that band diagrams for the 2D model of a LRM with multilayered cylindrical resonators are inappropriate to predict BG location for structures of a finite height due to the coupling between in-plane and out-of-plane modes. In practice, this means that the 2D results only make sense if one ensures that only one type of the modes is excited; however, mode coupling can still be triggered at the sample boundaries. In general, theoretical predictions based on 2D simulations for locally resonant metamaterials must be interpreted with caution.

3 Spherical Resonators

In this section, a metamaterial is considered that is composed by a square array of multilayered concentric spheres with a stiff core and alternating layers of stiff and compliant materials. A
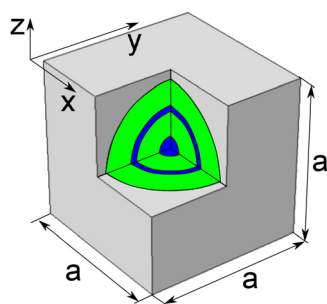
representative unit cell is shown in Fig. 4. The material parameters for the constituents and the geometrical dimensions are the same as those in Sec. 2, (see Fig. 1(*b*)). To model elastic waves propagating in the *XY* plane, standard Bloch boundary conditions are applied at the faces normal to *x* and *y* axes. At the two remaining faces, either traction-free or periodic (continuity) boundary conditions can be applied to model slab or infinite periodic metamaterial geometries, respectively. In this way, the influence of boundary conditions on the metamaterial wave dispersion can be analyzed. Dispersion diagrams are evaluated using 3D finite-element models with ca. 95,000 tetrahedral elements in COMSOL MULTIPHYSICS 5.0.

Figures 5(*a*) and 5(*b*) show the band diagrams for the considered metamaterial with free and periodic boundary conditions, respectively. For both cases, two closely located BGs exist at approximately the same frequencies as for the 2D in-plane modes (see Fig. 2(*b*)). The differences in BG frequencies for the 2D and 3D cases are attributed to different volume fractions of compliant and stiff materials for the same cross-sectional geometric parameters resulting in the shift of the resonator eigenfrequencies. In contrast to the case of cylindrical resonators shown in Fig. 3(*a*), the band diagrams in Figs. 5(*a*) and 5(*b*) reveal a smaller number of bands, since the frequencies corresponding to the 2D out-of-plane modes are completely absent in the case of spherical resonators.
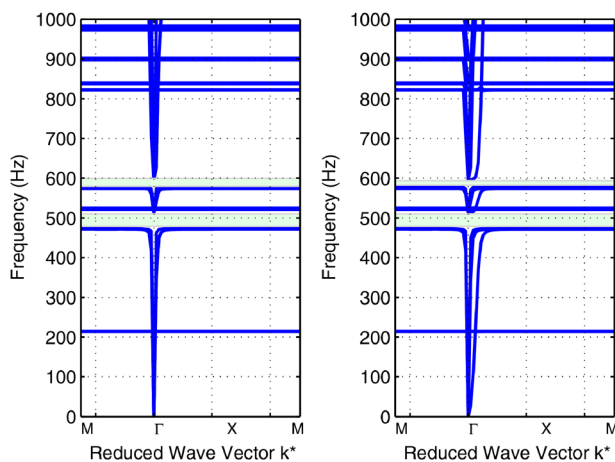

Fig. 4 Schematic representation of a 3D unit cell for an LRM with multilayered spherical inclusions

Fig. 5 Band diagrams for the metamaterial shown in Fig. 4 with (*a*) periodic and (*b*) traction-free boundary conditions at the faces normal to the *z* axis, respectively

By comparing the two diagrams, it is obvious that in the case of free boundaries, the modes approach their asymptotic values slower, as the value of the wave vector increases. This also results in a slightly smaller width of the second BG around 600 Hz. In general, the analyzed boundary conditions do not really influence the band structure diagrams. Hence, one may conclude that wave dispersion in 3D slab and 2D infinite metamaterial structures with multilayered spherical inclusions are almost indistinguishable. This conclusion is unexpected, since usually slab geometries reveal more complicated dispersion properties, accompanied by additional pass bands due to wave scattering at free boundaries.

The obtained results show that dispersion properties of 3D LRM with multilayered spherical inclusions can be correctly approximated by the 2D in-plane modes of the metamaterial central cross section. Thus, the conclusion derived by Liu et al. [11] for a case of a stiff spherical resonator coated with a rubber layer remains valid for multilayered resonators. This allows to reduce the simulation time and computation costs significantly. Moreover, it offers a quick and reasonably good estimate of the BG frequencies of these 3D structures.

4 Conclusions

In this letter, we studied the elastic wave propagation in 2D and 3D LRMs with multilayered resonators and found that the theoretical predictions based on 2D simulations, widely used in the literature, must be interpreted with caution. The wave dispersion in 3D metamaterial structures was found to be strongly influenced by the resonator's shape. Entirely different behaviors were observed for the resonators of a cylindrical and spherical shape with the same metamaterial midplane cross section. Three-dimensional slab structures with cylindrical dual resonators possess only one BG (in contrast to the expected double BGs given by the 2D analysis). Moreover, the BG bound frequencies have been shown to depend strongly on the height/width ratios that cannot be predicted by 2D models neglecting the resonator height. This result is analogous to the one known for slab phononic crystals. For spherical resonators, the wave dispersion and BG frequencies can be adequately described by using in-plane modes of the 2D approximation. Moreover, it was found that wave characteristics are almost indistinguishable for 3D slab and 2D infinite metamaterial geometries with spherical resonators. This result may facilitate the modeling of the computationally expensive 3D LRMs with multiple resonators.

References

[1] Molerón, M., and Daraio, C., 2015, "Acoustic Metamaterial for Subwavelength Edge Detection," Nat. Commun., 6, p. 8037.

[2] Miniaci, M., Krushynska, A., Bosia, F., and Pugno, N., 2016, "Large Scale Mechanical Metamaterials as Seismic Shields," New J. Phys., 18(8), p. 083041.

[3] Zigoneanu, L., Popa, B.-I., and Cummer, S., 2014, "Three-Dimensional Broadband Omnidirectional Acoustic Ground Cloak," Nat. Mater., 13(4), pp. 352–355.

[4] Larabi, H., Pennec, Y., Djafari-Rouhani, B., and Vasseur, J. O., 2007, "Multicoaxial Cylindrical Inclusions in Locally Resonant Phononic Crystals," Phys. Rev. E, 75(6), p. 066601.

[5] Tan, K., Huang, H., and Sun, C., 2014, "Blast-Wave Impact Mitigation Using Negative Effective Mass Density Concept of Elastic Metamaterials," Int. J. Impact Eng., 64, pp. 20–29.

[6] Chen, Y., Barnhart, M., Chen, J., Hu, G., Sun, C., and Huang, G., 2016, "Dissipative Elastic Metamaterials for Broadband Wave Mitigation at Subwavelength Scale," Compos. Struct., 136, pp. 358–371.

[7] Zhu, R., Liu, X., Hub, G., Sun, C., and Huang, G., 2014, "A Chiral Elastic Metamaterial Beam for Broad Band Vibration Suppression," J. Sound Vib., 333(10), pp. 2759–2773.

[8] Elford, D., Chalmers, L., Kusmartsev, F., and Swallowe, G., 2011, "Matryoshka Locally Resonant Sonic Crystal," J. Acoust. Soc. Am., 130(5), pp. 2746–2755.

[9] Krödel, S., Thomé, N., and Daraio, C., 2015, "Wide Band-Gap Seismic Metastructures," Extreme Mech. Lett., 4, pp. 111–117.

[10] Khelif, A., Aoubiza, B., Mohammadi, S., Adibi, A., and Laude, V., 2006, "Complete Band Gaps in Two-Dimensional Phononic Crystal Slabs," Phys. Rev. E, 74(4), p. 046610.

[11] Liu, Z., Chan, C., and Sheng, P., 2005, "Analytic Model of Phononic Crystals With Local Resonances," Phys. Rev. B, 71(1), p. 014103.

[12] Hirsekorn, M., Delsanto, P., Leung, A., and Matic, P., 2006, "Elastic Wave Propagation in Locally Resonant Sonic Material: Comparison Between Local Interaction Simulation Approach and Modal Analysis," J. Appl. Phys., 99(12), p. 124912.

[13] Hussein, M., Leamy, M., and Ruzzene, M., 2014, "Dynamics of Phononic Materials and Structures: Historical Origins, Recent Progress, and Future Outlook," ASME Appl. Mech. Rev., 66(4), p. 040802.

[14] Krushynska, A., Kouznetsova, V., and Geers, M., 2014, "Towards Optimal Design of Locally Resonant Acoustic Metamaterials," J. Mech. Phys. Solids, 71, pp. 179–196.

---

[2]http://www.hpc.polito.it